# Daytime Top-of-the-Atmosphere Cirrus Cloud Radiative Forcing Properties at Singapore

SIMONE LOLLI,[a,b] JAMES R. CAMPBELL,[c] JASPER R. LEWIS,[a] YU GU,[d] JARED W. MARQUIS,[e] BOON NING CHEW,[f] SOO-CHIN LIEW,[g] SANTO V. SALINAS,[g] AND ELLSWORTH J. WELTON[h]

[a] *Joint Center for Earth Systems Technology, University of Maryland, Baltimore County, Baltimore, Maryland*
[b] *Consiglio Nazionale Delle Ricerche, Istituto di Metodologie per l'Analisi Ambientale, Potenza, Italy*
[c] *Naval Research Laboratory, Monterey, California*
[d] *University of California, Los Angeles, Los Angeles, California*
[e] *University of North Dakota, Grand Forks, North Dakota*
[f] *Meteorological Service Singapore, Singapore*
[g] *Centre for Remote Imaging Sensing and Processing, National University of Singapore, Singapore*
[h] *NASA Goddard Space Flight Center, Greenbelt, Maryland*

(Manuscript received 27 July 2016, in final form 30 November 2016)

ABSTRACT

Daytime top-of-the-atmosphere (TOA) cirrus cloud radiative forcing (CRF) is estimated for cirrus clouds observed in ground-based lidar observations at Singapore in 2010 and 2011. Estimates are derived both over land and water to simulate conditions over the broader Maritime Continent archipelago of Southeast Asia. Based on bookend constraints of the lidar extinction-to-backscatter ratio (20 and 30 sr), used to solve extinction and initialize corresponding radiative transfer model simulations, relative daytime TOA CRF is estimated at 2.858–3.370 W m$^{-2}$ in 2010 (both 20 and 30 sr, respectively) and 3.078–3.329 W m$^{-2}$ in 2011 and over water between −0.094 and 0.541 W m$^{-2}$ in 2010 and −0.598 and 0.433 W m$^{-2}$ in 2011 (both 30 and 20 sr, respectively). After normalizing these estimates for an approximately 80% local satellite-estimated cirrus cloud occurrence rate, they reduce in absolute daytime terms to 2.198–2.592 W m$^{-2}$ in 2010 and 2.368–2.561 W m$^{-2}$ in 2011 over land and −0.072–0.416 W m$^{-2}$ in 2010 and −0.460–0.333 W m$^{-2}$ in 2011 over water. These annual estimates are mostly consistent despite a tendency toward lower relative cloud-top heights in 2011. Uncertainties are described. Estimates support the open hypothesis of a meridional hemispheric gradient in cirrus cloud daytime TOA CRF globally, varying from positive near the equator to presumably negative approaching the non-ice-covered poles. They help expand upon the paradigm, however, by conceptualizing differences zonally between overland and overwater forcing that differ significantly. More global oceans are likely subject to negative daytime TOA CRF than previously implied.

## 1. Motivation

Campbell et al. (2016) isolate top-of-atmosphere (TOA) net cirrus cloud radiative forcing (CRF) properties for a continuous 1-yr, single-layer cloud dataset developed from NASA ground-based Micro-Pulse Lidar Network (MPLNET; http://mplnet.gsfc.nasa.gov/) (Welton et al. 2001; Campbell et al. 2002; Lolli et al. 2013) observations collected at Greenbelt, Maryland [38.99°N, 76.84°W; 50 m above mean sea level (MSL)]. They estimate that cirrus clouds exert an absolute net positive daytime TOA CRF of 0.03–0.27 W m$^{-2}$ annually there, albeit with caveats related to the observational limitations of zenith-pointing ground-based lidars. They propose, however, that this slight positive daytime TOA CRF represents an approximate middle point in a meridional/hemispheric gradient of daytime cirrus TOA CRF, whereby higher/colder cirrus illuminated at endemically lower solar zenith angles (SZA) approaching the equator induce increasingly positive daytime TOA CRF as compared with lower/warmer cirrus illuminated at consistently higher SZA nearing the poles that likely yield negative daytime TOA CRF.

Whereas daytime TOA CRF gradients presumably exist for all clouds with latitude, primarily as a function

Denotes content that is immediately available upon publication as open access.

*Corresponding author e-mail*: Simone Lolli, simone.lolli@nasa.gov

DOI: 10.1175/JAMC-D-16-0262.1

of varying SZA characteristics, cirrus are unique for they are the only genus that, in isolation, can readily induce positive or negative daytime TOA CRF based on their widely varying physical characteristics [i.e., cloud heights, temperatures, effective particle sizes, surface thermal contrast, and ice water path/cloud optical depth; e.g., Stephens and Webster (1981)]. Other cloud genera induce negative daytime TOA CRF exclusively, cooling the daytime surface/atmospheric system below them. All clouds cause positive TOA CRF at night (i.e., a positive infrared term with no compensating negative solar component). Discovery of such a gradient, with fluctuating positive/negative daytime TOA CRF, would reveal a unique, yet fundamental, component of the atmospheric radiation budget that to date has gone unrecognized, a result of advanced cloud monitoring capabilities from ground and satellite lidar observations unavailable only 15 years prior.

Here, a 2-yr (2010–11) MPLNET dataset collected at the National University of Singapore (1.30°N, 103.77°E; 79 m MSL) is investigated for cirrus cloud daytime TOA CRF properties. Though complimentary, this study is unique relative to Campbell et al. (2016) in two ways: first, consecutive years are analyzed to investigate interannual variability in cirrus macrophysical and radiative properties; second, since Singapore is an island situated within the larger Maritime Continent archipelago, daytime TOA CRF estimates are solved both years as a function of overland and overwater surface albedos, a term that influences the solar contribution to TOA CRF and thus the net value overall. As such, these results more appropriately represent the practical system variance present within broader Southeast Asia. Estimates are further subset seasonally to investigate intra-annual variability. Campbell et al. (2016) hypothesize that the strongest meridional forcing gradients occur during respective summer hemispheric seasons (i.e., lesser ice coverage and more sunlight daily near the poles suppresses the solar forcing term and lowers relative net daytime TOA CRF regionally). These results will therefore establish important context near the equator for understanding the magnitude of such gradients.

## 2. Cirrus daytime TOA CRF at Singapore (2010–11)

### a. Experimental design

Campbell et al. (2016) describe the methodology applied to MPLNET data for estimating cirrus cloud daytime TOA CRF. Briefly, single-layer cirrus clouds are resolved according to Campbell et al. (2008, 2015) and Lewis et al. (2016). Radiative transfer calculations are performed using the Fu–Liou–Gu model (FLG; Fu and Liou 1992, 1993; Gu et al. 2003, 2011), featuring advanced parameterization of ice microphysical and optical properties (Yang et al. 2000, 2005) and a relationship between ice crystal radius and cloud-top-height-collocated NASA Goddard Modeling and Assimilation Office, version 5.9.1 (GEOS-5; http://gmao.gsfc.nasa.gov/products), reanalysis temperatures derived by Heymsfield et al. (2014) that is defined as a function of the lidar-derived extinction coefficient. The latter term is solved in unconstrained MPLNET retrievals using a priori settings for the lidar extinction-to-backscatter ratio (the so-called lidar ratio) of 20 and 30 sr to simulate practical bookend system variance (e.g., Chew et al. 2011; Garnier et al. 2015). GEOS-5 thermodynamic profiles are further used to initialize FLG simulations. One change to the modeling system comes from adding a varying ocean surface albedo term designed for accommodating very low solar zenith angles in the tropics and potential sun glint over water (Jin et al. 2004).

Clouds are modeled assuming particulate aerosol- and cloud-free skies above and below so as to isolate the cirrus TOA CRF term. Whereas cirrus clouds often occur with other clouds present, the point is to characterize their distinct forcing effect. Further, daytime hours are uniquely defined within the model as those where incoming clear-sky insolation exceeds net outgoing energy at the TOA. This is a reasonable approximation to the critical minimum insolation threshold by which clouds can potentially induce positive or negative daytime TOA CRF [for more details, see Campbell et al. (2016), though they forget to add surface albedo as a term that can influence the absolute value]. Otherwise, conditions are effectively that of nighttime whereby all clouds can induce only positive values. A summary of all primary experimental and data-related elements applied in this study is outlined in Table 1, although the reader is again referred to Campbell et al. (2016) for greater detail on how these components are motivated.

### b. Results and discussion

Figure 1 depicts absolute cirrus cloud frequencies over water throughout Southeast Asia and the Maritime Continent derived from 2006–15 satellite-based Cloud–Aerosol Lidar with Orthogonal Polarization (CALIOP; Winker et al. 2010), level-2, 5-km cloud profile datasets. Cirrus are defined here, as with MPLNET, based on a maximum −37°C cloud-top temperature, as advocated in Campbell et al. (2015). Total cirrus cloud occurrence near Singapore approaches 80% (Fig. 1a). Following Sassen and Cho (1992), over half of these clouds are translucent: optically thin cirrus (OTC) exceed 30%

TABLE 1. A summary listing of primary experimental components and data constraints used in this study.

| Experimental component | Selection | References (if applicable) |
|---|---|---|
| Radiative transfer model | FLG $\delta$-four stream system | Fu and Liou (1992, 1993); Gu et al. (2003) |
| Ice single-scattering and absorption properties | — | Yang et al. (2000; solar); Yang et al. (2005; infrared) |
| Model meteorological conditions | GEOS-5 | http://gmao.gsfc.nasa.gov/products |
| Surface albedo | MODIS monthly averaged broadband values | Strahler et al. (1999) |
| Land surface thermal emissivity | 0.97 | Jin and Liang (2006) |
| Ice microphysical parameterization | — | Heymsfield et al. (2014) |
| Definition for daytime hours | Incoming clear-sky TOA solar radiation exceeds outgoing | — |
| Cirrus cloud dataset | MPLNET, version 3.0, cloud product | Campbell et al. (2008); Lewis et al. (2016); http://mplnet.gsfc.nasa.gov/ |
| Cirrus cloud thermal constraints | CTH temperature $\leq -37$°C | Campbell et al. (2015) |

occurrence [Fig. 1b; 0.03 $\leq$ cloud optical depth (COD) $<$ 0.30], while subvisual cloud (SVC) occurrence (COD $<$ 0.03) is only slightly lower (Fig. 1c).

Absolute and relative single-layer annual and monthly cirrus cloud occurrence rates during 2010 and 2011 in MPLNET observations at Singapore are listed in Fig. 2 alongside histograms of relative occurrence as a function of cloud-top height (CTH) and COD for the 30-sr sample. The Singapore MPL operated on 357 and 363 days in 2010 and 2011, respectively. 15 208 (8% absolute frequency) and 18 234 (10%) single-layer clouds were analyzed for daytime TOA CRF each respective year. Seasonal stats and histograms are shown for February–April (FMA; 3770 and 3920), May–July (MJJ; 4656 and 6594), September–November (SON; 4085 and 5179), and December–February (DJF; 2897 and 2541). Total cirrus cloudiness (i.e., single and multilayer) was 28% and 27%, respectively, varying in height between 10 and 18 km MSL. Relative sample distributions versus COD were consistent across both years: 16%/15% SVC, 64%/65% OTC + SVC, and 35%/35% COD $>$ 0.30. There was a distinct tendency, however, toward lower CTH during 2011 (14.09-km average CTH in 2010 vs 13.45 km in 2011).

Consideration of single-layer cirrus cloud subsets limits the potential for signal attenuation effects and aliasing of upper-cloud-layer features. Additional constrains on the data sample are present. For instance, as compared with the 40/60 distribution in daytime versus nighttime profiles at the Greenbelt, Maryland, site investigated in Campbell et al. (2016), Singapore experienced a 45/55 split across both 2010 and 2011 (presumably because of frequently lower SZA). Unlike the former sample, however, where an equal 40/60 split was detected in relative cloud occurrence, a 30/70 split was found at Singapore between day and night. This implies day/night cloud sampling bias present, either from lower daytime instrument sensitivity or greater low cloudiness during day that inhibited regular profiling of the upper troposphere. Further to this point, though it likely does not reconcile the full effect, a shutter was used to protect the instrument from extremely low solar zenith angles incident near solar noon on site. The instrument was thus in standby mode for approximately 60 min centered on solar noon each day, the *lidar siesta time* of the tropics (Sassen et al. 2005).

We also note that the approximately 65/35 split in optically thin and subvisual versus opaque clouds in this sample, as derived from the 30-sr sample introduced above and denoted in Figs. 2a and 2f, is consistent with the corresponding distribution observed by Campbell et al. (2016) at Greenbelt. It is thus very likely that sampling bias toward thinner clouds is present here, as a result, as these splits are believed disproportionately high (e.g., Sassen and Campbell 2001; Campbell et al. 2015). Campbell et al. (2016) inventory and describe further the sources of uncertainty arising within the experimental design applied here, primarily through observational concerns relating to ground-based profiling of the upper troposphere introduced by Thorsen et al. (2011) and Protat et al. (2014). The net TOA CRF results reported are strictly estimates within the bounds of resolvable experimental variance.

Shown in Fig. 3 are frequency-normalized daytime TOA CRF estimates solved as functions of COD and lidar ratio, including relative occurrence frequency, from 2010 and 2011. Complementary solutions are shown, reflecting a varying broadband solar surface albedo term that reconciles the cloud forcing effect over land (0.12 surface albedo; Figs. 3a,c) and over open waters (0.05; Figs. 3b,d; Strahler et al. 1999). Cirrus cloud relative occurrence exponentially

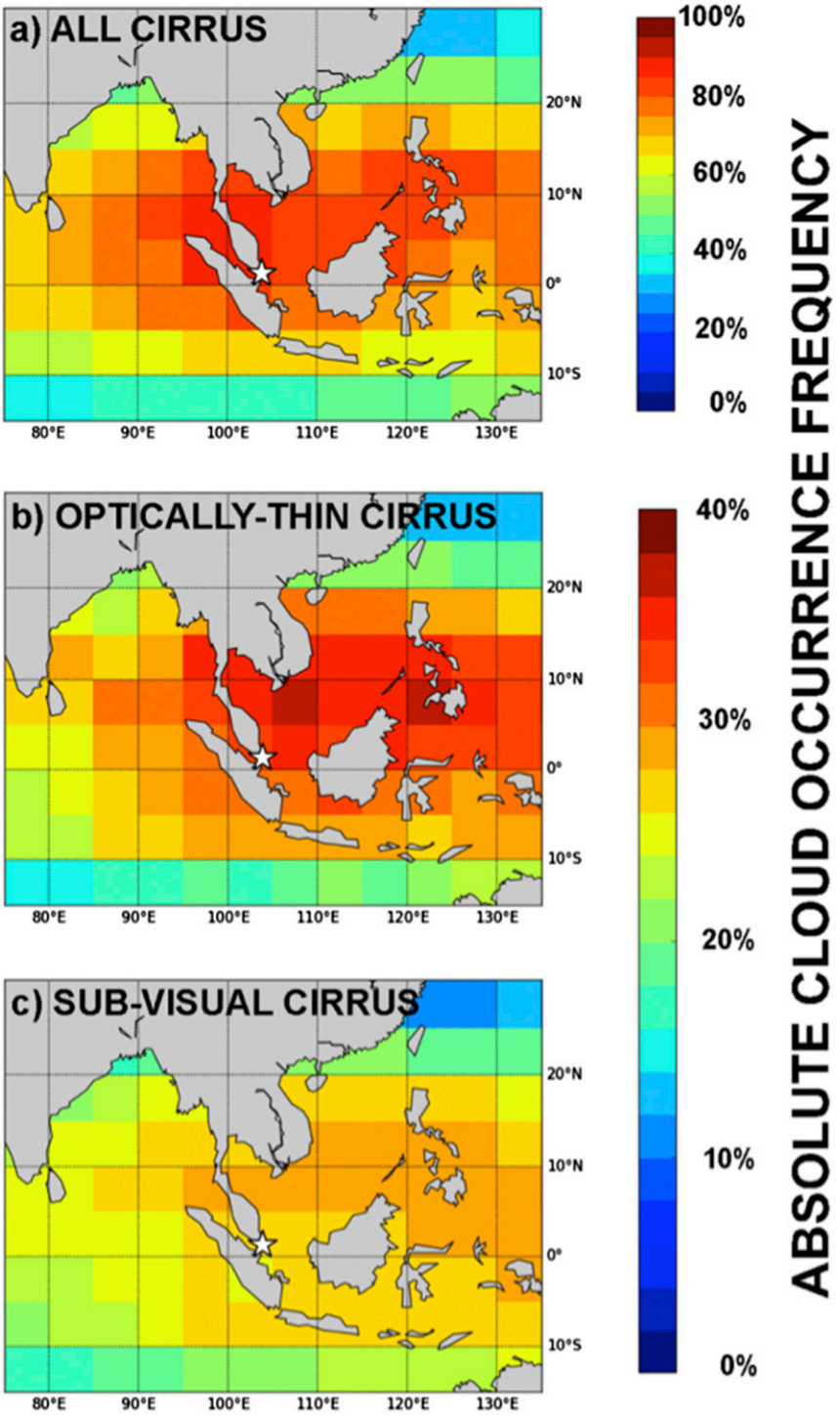


FIG. 1. Annual cirrus cloud absolute occurrence frequencies over the Southeast Asian Maritime Continental basin derived from level-2 NASA CALIOP 5-km cloud profile data products from 2006 to 2015 for all (a) cirrus clouds (see text for specific definition), (b) optically thin cirrus ($0.03 \leq \text{COD} < 0.30$), and (c) subvisual cirrus ($\text{COD} \leq 0.03$). Singapore is denoted by the star.

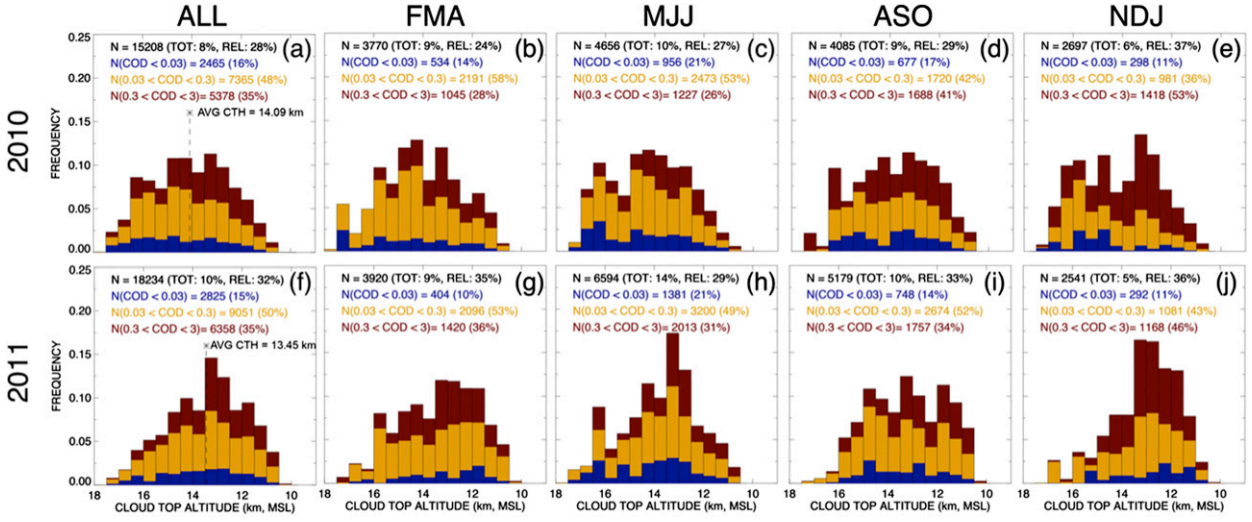


FIG. 2. Annual and seasonal relative cirrus cloud occurrence histograms for MPLNET observations at Singapore during (top) 2010 and (bottom) 2011 vs CTH, drawn as functions of COD (30-sr solutions shown only) with corresponding absolute and relative occurrence frequencies and mean average annual CTH (see insets): (a),(f) annual; (b),(g) FMA; (c),(h) MJJ; (d),(i) August–October (ASO); (e),(j) NDJ.

increases with decreasing COD, consistent with other studies (e.g., Campbell et al. 2015). TOA CRF values normalized by these occurrence rates reflect distributions where the most significant forcing effect is proportioned accordingly toward such clouds (Berry and Mace 2014). Since a common cloud sample is used for both the 20- and 30-sr samples, a maximum cirrus cloud COD = 3.00 was imposed (i.e., Sassen and Cho 1992), causing a maximum corresponding value at 20 sr near 0.75.

Relative daytime TOA CRF over land varied between 2.858 and 3.370 $W\,m^{-2}$ (20 and 30 sr, respectively) in 2010 and 3.078 and 3.329 $W\,m^{-2}$ in 2011, and over water between −0.094 and 0.541 $W\,m^{-2}$ in 2010 (30 and 20 sr,

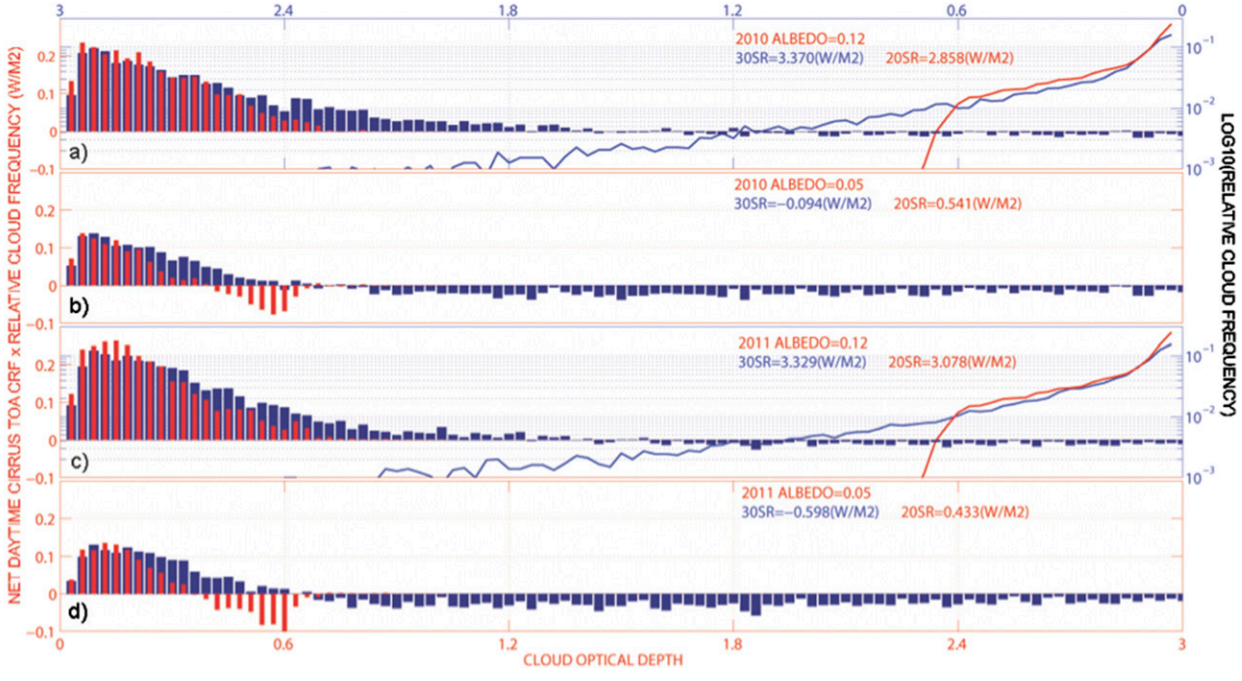


FIG. 3. Cirrus cloud frequency-normalized TOA CRF (left axis; red) vs COD at Singapore. Estimates are shown for both the 20- (red) and 30-sr (dark blue) bookend estimates to the lidar extinction-to-backscatter ratio for (top), (top middle) 2010 and (bottom middle), (bottom) 2011 over (a),(c) water and (b),(d) land, including corresponding relative cloud frequency (log10 based) vs COD (right axis; light blue).

TABLE 2. Seasonal relative net TOA cirrus CRF estimates at Singapore ($W m^{-2}$), solved as function of varying surface albedo, lidar ratio solutions for MPLNET cloud extinction, and year.

| | FMA | | | | MJJ | | | | ASO | | | | NDJ | | | |
|---|---|---|---|---|---|---|---|---|---|---|---|---|---|---|---|---|
| Surface albedo | 0.05 | | 0.12 | | 0.05 | | 0.12 | | 0.05 | | 0.12 | | 0.05 | | 0.12 | |
| *S* ratio (sr) | 20 | 30 | 20 | 30 | 20 | 30 | 20 | 30 | 20 | 30 | 20 | 30 | 20 | 30 | 20 | 30 |
| 2010 ($W m^{-2}$) | 1.13 | 0.82 | 3.14 | 3.78 | 0.75 | 0.55 | 2.62 | 3.28 | 0.14 | −0.72 | 2.76 | 3.18 | −0.11 | −1.52 | 2.83 | 3.83 |
| 2011 ($W m^{-2}$) | 0.94 | −0.32 | 3.82 | 4.01 | 0.94 | 0.61 | 3.07 | 3.74 | 0.51 | −0.38 | 3.08 | 3.43 | −1.97 | −4.51 | 1.57 | 0.72 |

respectively) and −0.598 and 0.433 $W m^{-2}$ in 2011; the difference being the impact of lower surface albedo over water that suppresses the relative solar forcing component within the net solutions. In absolute terms, given the nearly 80% regional cirrus occurrence frequency from satellite, and thus normalizing the results by approximately 1.3, these estimates become 2.198–2.592 $W m^{-2}$ in 2010 and 2.368–2.561 $W m^{-2}$ in 2011 over land, and −0.072–0.416 $W m^{-2}$ in 2010 and −0.460–0.333 $W m^{-2}$ in 2011 over water.

Missing observations near solar noon impact the overwater estimates more significantly than those over land. Each of the estimates is offset low to some degree specifically because of this aspect of the sampling bias believed present, since extremely low SZA cases correspond with positive net daytime TOA CRF (see below). However, overwater estimates are more sensitive, since model albedo is now designed to increase at the very lowest SZA from sun glint that increases the solar TOA CRF component and corresponding net estimate. Still, despite the CTH shift between 2010 and 2011, the annual estimates are relatively consistent. Given the varying dynamic mechanisms regionally that influence convection, and presumably cirrus cloud macrophysical properties (e.g., Zhang 2013), this result is noteworthy.

Seasonal daytime TOA CRF estimates are shown in Table 2, again over land/water, interannually and for each of the 20- and 30-sr samples. Given the variance apparent, it is difficult to definitively characterize any trends. November–January (NDJ) stands out for exhibiting exclusively net negative daytime TOA CRF over water during both years, however, whereas MJJ is the only overwater period where the estimates are all positive. The former corresponds with a distinct shift toward lower CTH in 2011, in particular, seen from Fig. 2j. Over land, NDJ estimates are also collectively the lowest, albeit within the margin of relative uncertainty.

It is compelling that the minimum 30-sr estimate over water in 2011 (−4.51 $W m^{-2}$; NDJ) stands in direct contrast with the maximum 30-sr estimate that year over land (4.01 $W m^{-2}$; FMA). Considering the overland/water estimates seasonally in tandem with the net annual estimates from Fig. 3, and notwithstanding the hypothetical presence of a meridional/hemispheric gradient in forcing [though these results reinforce the likelihood of such a phenomenon relative to the midlatitude estimates in Campbell et al. (2016)], it is apparent that there exist additional zonal gradients in cirrus cloud net daytime TOA CRF induced by dominant surface type. Whereas Campbell et al. (2016) recognize this process meridionally relative to polar ice coverage, they underestimate the simpler difference between land and open waters. Further, though they report slightly positive midlatitude values over land, the nature of the gradient appears fundamentally different over water. Given the slightly positive estimates over water at Singapore, cirrus likely induce negative daytime TOA CRF over much of the global oceans, presuming forcing turns negative meridionally at a lower latitude than over land.

Shown in Fig. 4 are frequency-normalized daytime TOA CRF and relative cloud frequency for each year and lidar ratio sample versus SZA. Figure 5 is similar to Fig. 4, but versus CTH instead of SZA. Relative distributions versus SZA are consistent across both years, which imply no daytime sampling bias on the results except for the minimum SZA of only about 8° caused by the instrument standby period around solar noon. Crossover points between positive and negative TOA CRF occur near 60° over land and 45° over water. Differences in relative occurrence versus CTH are more clearly apparent. Yet, aside from minor differences in normalized TOA CRF approaching −80°C, the distributions overall are similar, which is consistent with the nature of the annual bulk estimates. Crossover points between positive and negative TOA CRF occur near −45°C over land and −55°C over water. This overland crossover value is slightly warmer than that observed in the MPLNET midlatitude study, while SZA is slightly higher (Campbell et al. 2016), suggesting that some latitudinal variation is likely with respect to both parameters and their apparent crossover thresholds.

## 3. Conclusions

Daytime top-of-the-atmosphere cirrus cloud radiative forcing is estimated for single-layer cirrus clouds observed at a NASA ground-based Micro-Pulse Lidar Network site at Singapore in 2010 and 2011. Solutions are derived both over land and water (i.e., varying surface albedos) to simulate conditions both on the island

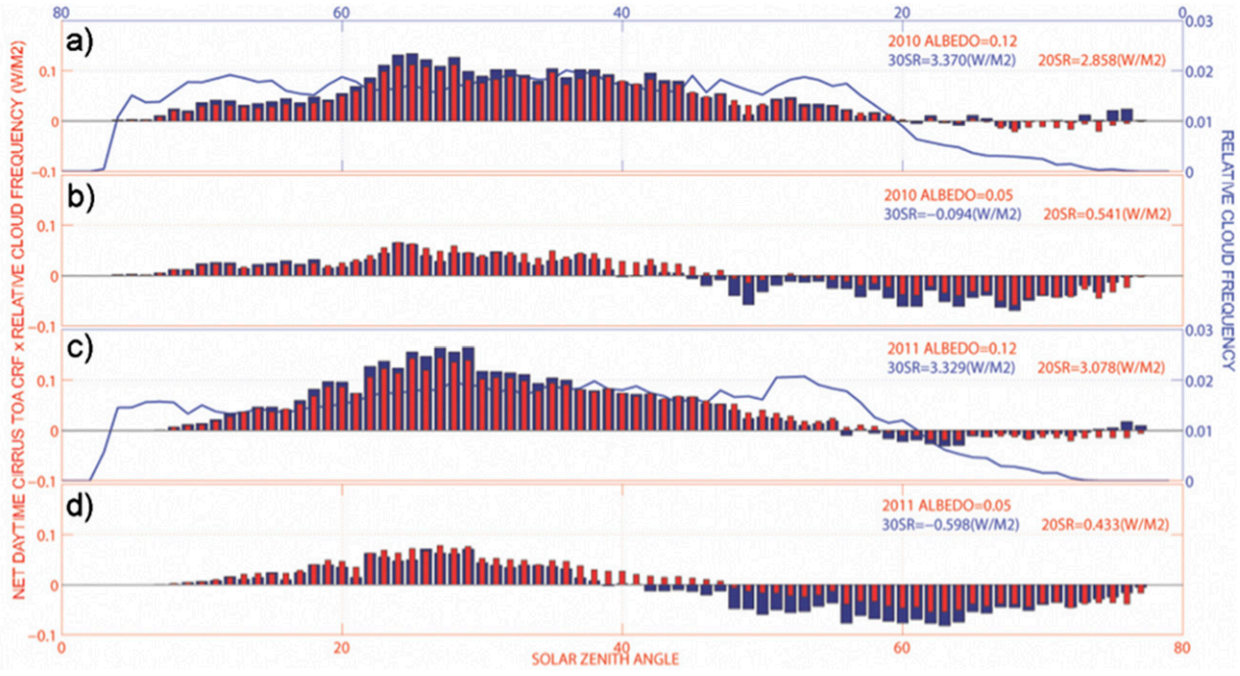


FIG. 4. As in Fig. 3, but vs SZA and relative cloud frequencies in (a) and (c) are plotted linearly.

and over the broader Southeast Asian Maritime Continent archipelago. Based on bookend solutions to the lidar extinction-to-backscatter ratio (20 and 30 sr), necessary to derive the dependent value (extinction) used to initialize radiative transfer model simulations, relative TOA CRF is estimated at 2.858–3.370 W m$^{-2}$ in 2010 (both 20 and 30 sr, respectively) and 3.078–3.329 W m$^{-2}$ in 2011, and over water between −0.094 and 0.541 W m$^{-2}$ in 2010 and −0.598 and 0.433 W m$^{-2}$ in 2011 (both 30 and 20 sr, respectively). When

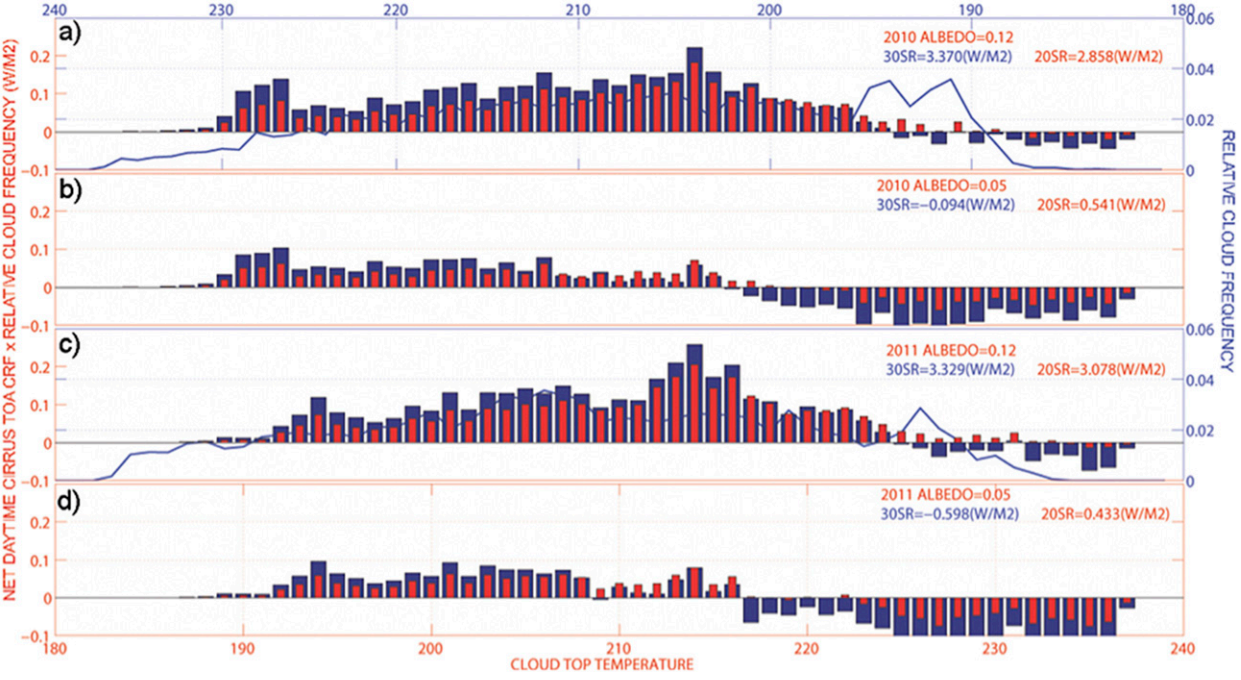


FIG. 5. As in Fig. 3, but vs CTH and relative cloud frequencies in (a) and (c) are plotted linearly.

normalized for an approximately 80% local cirrus cloud frequency, estimated from satellite, these values reduce in absolute terms to 2.198–2.592 $W m^{-2}$ in 2010 and 2.368–2.561 $W m^{-2}$ in 2011 over land, and $-0.072$–$0.416 W m^{-2}$ in 2010 and $-0.460$–$0.333 W m^{-2}$ in 2011 over water. Annual TOA CRF estimates are relatively consistent despite lower cloud-top heights observed in 2011 relative to 2010. Seasonal estimates are also mostly consistent as well, though the November–January period exhibits values that are slightly lower over both land and water relative to other months.

Relative uncertainties in these estimates relating to the experimental design are described. The results are believed to be slightly low because of the instrument being placed in standby mode for 60 min each day centered on solar noon to protect it from hazardous low solar zenith angles, which limits some corresponding strongly positive TOA CRF cases in the sample. Further, a relative offset is found in cirrus cloud occurrence between day and night in the sample (30/70 occurrence for day vs night as compared with a 45/55 split in corresponding hours in the day found annually) that implies a sampling bias effect present, differing significantly from an equal 40/60 split in both occurrence and day/night hours found by Campbell et al. (2016) at Greenbelt. The cloud sample is further believed disproportionately represented by optically thinner clouds (cloud optical depths $\leq 0.30$; 65/35 optically thin vs opaque solved at 30 sr).

The study follows a midlatitude study of 2010 MPLNET cirrus cloud TOA radiative properties (Campbell et al. 2016). The novelty in isolating daytime cirrus cloud TOA CRF comes from cirrus being the only genus that can readily induce both positive and/or negative daytime TOA CRF depending on their physical characteristics. All other tropospheric clouds induce a negative daytime value and a positive one at night. By categorizing the frequency-normalized daytime TOA CRF versus SZA and CTH, Campbell et al. (2016) hypothesize a meridional hemispheric gradient in daytime TOA CRF, varying from positive at the equator, neutral in the midlatitudes, and negative near the non-ice-covered (i.e., summer) poles. Results from Singapore are consistent with the existence of such a gradient, with one fundamental exception: the significance of overland versus overwater albedos leads to complimentary zonal forcing gradients, a component that Campbell et al. (2016) did not recognize. This occurs as the solar component of daytime TOA CRF is suppressed relative to overland conditions, which leads to significantly lower net values overall. This study thus demonstrates the compelling likelihood that much of the global oceans are subject to negative daytime TOA CRF, presuming the forcing sign changes meridionally at lower latitudes than believed likely over land.

Subsequent merit in continuing investigation of cirrus TOA CRF properties, aside from evaluating the hypothesis of a daytime meridional CRF gradient oscillating around 0, is rooted in the goal of transitioning such knowledge into practical parameterization and/or verification for weather and climate models. Cirrus are the most common cloud in the atmosphere (e.g., Mace et al. 2009; Stubenrauch et al. 2013, and references therein). Though the net TOA CRF associated with any single cirrus cloud is often on the order of $1 W m^{-2}$, their impact on global radiation is grounded in the long-term aggregate, since they are nearly an order of magnitude more common than most liquid cloud genera that induce significantly greater TOA CRF. The inability of passive radiometers to monitor thin cirrus (e.g., Ackerman et al. 2008), for which nearly half of all cirrus exhibit an optical depth $< 0.30$ (Campbell et al. 2015), renders lidar observations compulsory in understanding their macrophysical and radiative properties. Whereas questions are outstanding with regards to reconciling TOA radiance budgets in both passive satellite observations and modeling initiatives (e.g., Waliser et al. 2009; Seiki et al. 2015), the ability to even conceptualize a meridional daytime forcing gradient, using practical estimates of its magnitude, proves a worthy goal for ongoing efforts with MPLNET and an eventual extrapolation of the current work to satellite cloud measurements.

*Acknowledgments.* The NASA Micro-Pulse Lidar Network is supported by the NASA Radiation Sciences Program (H. Maring). Author JRC acknowledges the support of the Naval Research Laboratory Base Program (BE033-03-45-T008-17) and NASA Interagency Agreement NNG15JA17P on behalf of MPLNET. The authors thank Jeffery S. Reid (Naval Research Laboratory) for supporting the instrument deployment to Singapore, which took place through the Seven Southeast Asian Studies program under the sponsorship in part of the Office of Naval Research (ONR) Code 322 and ONR Global. The authors acknowledge the contributions of the associate editor and our three colleagues who participated anonymously in peer review.

## REFERENCES

Ackerman, S. A., R. E. Holz, R. Frey, E. W. Eloranta, B. C. Maddux, and M. McGill, 2008: Cloud detection with MODIS. Part II: Validation. *J. Atmos. Oceanic Technol.*, **25**, 1073–1086, doi:10.1175/2007JTECHA1053.1.

Berry, E., and G. G. Mace, 2014: Cloud properties and radiative effects of the Asian summer monsoon derived from A-Train data. *J. Geophys. Res. Atmos.*, **119**, 9492–9508, doi:10.1002/2014JD021458.

Campbell, J. R., D. L. Hlavka, E. J. Welton, C. J. Flynn, D. D. Turner, J. D. Spinhirne, V. S. Scott, and I. H. Hwang, 2002: Full-time, eye-safe cloud and aerosol lidar observation at Atmosphere Radiation Measurement program sites: Instrument and data processing. *J. Atmos. Oceanic Technol.*, **19**, 431–442, doi:10.1175/1520-0426(2002)019<0431:FTESCA>2.0.CO;2.

——, K. Sassen, and E. J. Welton, 2008: Elevated cloud and aerosol layer retrievals from micropulse lidar signal profiles. *J. Atmos. Oceanic Technol.*, **25**, 685–700, doi:10.1175/2007JTECHA1034.1.

——, M. A. Vaughan, M. Oo, R. E. Holz, J. R. Lewis, and E. J. Welton, 2015: Distinguishing cirrus cloud presence in autonomous lidar measurements. *Atmos. Meas. Tech.*, **8**, 435–449, doi:10.5194/amt-8-435-2015.

——, S. Lolli, J. R. Lewis, Y. Gu, and E. J. Welton, 2016: Daytime cirrus cloud top-of-atmosphere radiative forcing properties at a midlatitude site and their global consequence. *J. Appl. Meteor. Climatol.*, **55**, 1667–1679, doi:10.1175/JAMC-D-15-0217.1.

Chew, B. N., J. R. Campbell, J. S. Reid, D. M. Giles, E. J. Welton, S. V. Salinas, and S. C. Liew, 2011: Tropical cirrus cloud contamination in sun photometer data. *Atmos. Environ.*, **45**, 6724–6731, doi:10.1016/j.atmosenv.2011.08.017.

Fu, Q., and K. N. Liou, 1992: On the correlated *k*-distribution method for radiative transfer in nonhomogeneous atmospheres. *J. Atmos. Sci.*, **49**, 2139–2156, doi:10.1175/1520-0469(1992)049<2139:OTCDMF>2.0.CO;2.

——, and ——, 1993: Parameterization of the radiative properties of cirrus clouds. *J. Atmos. Sci.*, **50**, 2008–2025, doi:10.1175/1520-0469(1993)050<2008:POTRPO>2.0.CO;2.

Garnier, A., J. Pelon, M. A. Vaughan, D. M. Winker, C. R. Trepte, and P. Dubuisson, 2015: Lidar multiple scattering factors inferred from *CALIPSO* lidar and IIR retrievals of semi-transparent cirrus cloud optical depths over oceans. *Atmos. Meas. Tech.*, **8**, 2759–2774, doi:10.5194/amt-8-2759-2015.

Gu, Y., J. Farrara, K. N. Liou, and C. R. Mechoso, 2003: Parameterization of cloud–radiation processes in the UCLA general circulation model. *J. Climate*, **16**, 3357–3370, doi:10.1175/1520-0442(2003)016<3357:POCPIT>2.0.CO;2.

——, K. N. Liou, S. C. Ou, and R. Fovell, 2011: Cirrus cloud simulations using WRF with improved radiation parameterization and increased vertical resolution. *J. Geophys. Res.*, **116**, D06119, doi:10.1029/2010JD014574.

Heymsfield, A., D. Winker, M. Avery, M. Vaughan, G. Diskin, M. Deng, V. Mitev, and R. Matthey, 2014: Relationships between ice water content and volume extinction coefficient from in situ observations for temperatures from 0° to −86°C: Implications for spaceborne lidar retrievals. *J. Appl. Meteor. Climatol.*, **53**, 479–505, doi:10.1175/JAMC-D-13-087.1.

Jin, M., and S. Liang, 2006: An improved land surface emissivity parameter for land surface models using global remote sensing observations. *J. Climate*, **19**, 2867–2881, doi:10.1175/JCLI3720.1.

Jin, Z., T. P. Charlock, W. L. Smith Jr., and K. Rutledge, 2004: A parameterization of ocean surface albedo. *Geophys. Res. Lett.*, **31**, L22301, doi:10.1029/2004GL021180.

Lewis, J. R., J. R. Campbell, E. J. Welton, S. A. Stewart, and P. C. Haftings, 2016: Overview of MPLNET, version 3, cloud detection. *J. Atmos. Oceanic Technol.*, **33**, 2113–2134, doi:10.1175/JTECH-D-15-0190.1.

Lolli, S., E. J. Welton, and J. R. Campbell 2013: Evaluating light rain drop size estimates from multiwavelength micropulse lidar network profiling. *J. Atmos. Oceanic Technol.*, **30**, 2798–2807, doi:10.1175/JTECH-D-13-00062.1.

Mace, G. G., Q. Zhang, M. Vaughan, R. Marchand, G. Stephens, C. Trepte, and D. Winker, 2009: A description of hydrometeor layer occurrence statistics derived from the first year of merged *CloudSat* and *CALIPSO* data. *J. Geophys. Res.*, **114**, D00A26, doi:10.1029/2007JD009755.

Protat, A., and Coauthors, 2014: Reconciling ground-based and space-based estimates of the frequency of occurrence and radiative effect of clouds around Darwin, Australia. *J. Appl. Meteor. Climatol.*, **53**, 456–478, doi:10.1175/JAMC-D-13-072.1.

Sassen, K., and B. S. Cho, 1992: Subvisual-thin cirrus lidar dataset for satellite verification and climatological research. *J. Appl. Meteor.*, **31**, 1275–1285, doi:10.1175/1520-0450(1992)031<1275:STCLDF>2.0.CO;2.

——, and J. R. Campbell, 2001: A midlatitude cirrus cloud climatology from the Facility for Atmospheric Remote Sensing. Part I: Macrophysical and synoptic properties. *J. Atmos. Sci.*, **58**, 481–496, doi:10.1175/1520-0469(2001)058<0481:AMCCCF>2.0.CO;2.

——, ——, J. Zhu, P. Kollias, M. Shupe, and C. Williams, 2005: Lidar and triple-wavelength Doppler radar measurements of the melting layer: A revised model for dark- and brightband phenomena. *J. Appl. Meteor.*, **44**, 301–312, doi:10.1175/JAM-2197.1.

Seiki, T., C. Kodama, M. Satoh, T. Hashino, Y. Hagihara, and H. Okamoto, 2015: Vertical grid spacing necessary for simulating tropical cirrus clouds with a high-resolution atmospheric general circulation model. *Geophys. Res. Lett.*, **42**, 4150–4157, doi:10.1002/2015GL064282.

Stephens, G. L., and P. J. Webster, 1981: Clouds and climate: Sensitivity of simple systems. *J. Atmos. Sci.*, **38**, 235–247, doi:10.1175/1520-0469(1981)038<0235:CACSOS>2.0.CO;2.

Strahler, A. H., and Coauthors, 1999: MODIS BRDF/albedo product: Algorithm Theoretical Basis Document. NASA EOS-MODIS Doc. ATBD-MOD-09, version 5.0, 53 pp. [Available online at https://modis.gsfc.nasa.gov/data/atbd/atbd_mod09.pdf.]

Stubenrauch, C. J., and Coauthors, 2013: Assessment of global cloud datasets from satellites. *Bull. Amer. Meteor. Soc.*, **94**, 1031–1049, doi:10.1175/BAMS-D-12-00117.1.

Thorsen, T. J., Q. Fu, and J. Comstock, 2011: Comparison of the *CALIPSO* satellite and ground-based observations of cirrus clouds at the ARM TWP sites. *J. Geophys. Res.*, **116**, D21203, doi:10.1029/2011JD015970.

Waliser, D., and Coauthors, 2009: Cloud ice: A climate model challenge with signs and expectations of progress. *J. Geophys. Res.*, **114**, D00A21, doi:10.1029/2008JD010015.

Welton, E. J., J. R. Campbell, J. D. Spinhirne, and V. S. Scott, 2001: Global monitoring of clouds and aerosols using a network of micro-pulse lidar systems. *Lidar Remote Sensing for Industry and Environmental Monitoring*, U. N. Singh, T. Itabe, and N. Sugimoto, Eds., International Society for Optical Engineering (SPIE Proceedings, Vol. 4153), 151–158.

Winker, D. M., and Coauthors, 2010: The *CALIPSO* mission: A global 3D view of aerosols and clouds. *Bull. Amer. Meteor. Soc.*, **91**, 1211–1229, doi:10.1175/2010BAMS3009.1.

Yang, P., K. N. Liou, K. Wyser, and D. Mitchell, 2000: Parameterization of the scattering and absorption properties of individual ice crystals. *J. Geophys. Res.*, **105**, 4699–4718, doi:10.1029/1999JD900755.

——, H. Wei, H.-L. Huang, B. A. Baum, Y. X. Hu, G. W. Kattawar, M. I. Mischenko, and Q. Fu, 2005: Scattering and absorption property database for nonspherical ice particles in the near-through far-infrared spectral region. *Appl. Opt.*, **44**, 5512–5523, doi:10.1364/AO.44.005512.

Zhang, C., 2013: Madden–Julian oscillation: Bridging weather and climate. *Bull. Amer. Meteor. Soc.*, **94**, 1849–1870, doi:10.1175/BAMS-D-12-00026.1.